Properties of light particles produced in Ar + Ni collisions at 95 A.MeV : evaporation versus prompt emission

D. Dore, C. Volant, J. Cugnon, R. Legrain, G. Auger, Ch-O. Bacri, N. Bellaize, B. Borderie, R. Bougault, B. Bouriquet, et al.

Institut de Physique Nucléaire de Lyon

Université Claude Bernard

IN2P3 - CNRS

LYCEN 2000/67
LPCC 00-013
August, 2000

Properties of light particles produced in Ar + Ni collisions at 95 A.MeV : evaporation versus prompt emission

D. Doré, et al.
INDRA Collaboration

Submitted to Nuclear Physics

43, Boulevard du 11 Novembre 1918 - 69622 VILLEURBANNE Cedex - France

Properties of light particles produced in Ar+Ni collisions at 95 A.MeV: Evaporation versus prompt emission.

D. Doré[1], C. Volant[1], J. Cugnon[2], R. Legrain[1], G. Auger[3], Ch. O. Bacri[4], N. Bellaize[5], B. Borderie[4], R. Bougault[5], B. Bouriquet[3], R. Brou[5], P. Buchet[1], J. L. Charvet[1], A. Chbihi[3], J. Colin[5], D. Cussol[5], R. Dayras[1] , A. Demeyer[6], D. Durand[5], J. D. Frankland[3], E. Galichet[4,9], E. Genouin-Duhamel[5], E. Gerlic[6], D. Guinet[6], B. Guiot[3], S. Hudan[3], P. Lautesse[6], F. Lavaud[4], J. L. Laville[3], J. F. Lecolley[5], C. Leduc[6], N. LeNeindre[5], O. Lopez[5], M. Louvel[5], A. M. Maskay[6], L. Nalpas[1], J. Normand[5], P. Pawłowski[4], M. Pârlog[7], E. Plagnol[4], M. F. Rivet[4], E. Rosato[8], F. Saint-Laurent[3,*] , J. C. Steckmeyer[5], G. Tăbăcaru[7], B. Tamain[5], L. Tassan-Got[4], E. Vient[5], J. P. Wieleczko[3]

(INDRA Collaboration)

(1) DAPNIA/SPhN, CEA/Saclay, 91191 Gif-sur-Yvette Cedex, France

(2) University of Liège, Physics Department, B5, B-4000 Sart-Tilman Liège 1, Belgium

(3)GANIL (DSM-CEA/IN2P3-CNRS), B.P. 5027, 14076 Caen Cedex 5, France

(4)IPN Orsay (IN2P3-CNRS), 91406 Orsay Cedex, France

(5)LPC Caen (IN2P3-CNRS/ISMRA et Université), 14050 Caen Cedex , France

(6)IPN Lyon (IN2P3-CNRS/Université), 69622 Villeurbanne Cedex, France

(7)Nuclear Institute for Physics and Nuclear Engineering, Bucharest, Romania

(8)Dipartimento di Scienze Fisiche, Univ. di Napoli, 80126 Napoli, Italy

(9)Conservatoire National des Arts et Métiers, 75141 Paris Cedex 03, France.

(June 30, 2000)

Abstract

Intermediate velocity emissions of light charged particles are studied for the

*present address : CEA, DRFC/STEP, CE Cadarache, 13108 Saint-Paul-lez-Durance, France

Ar + Ni system at 95 A.MeV. Experimental parallel velocity distributions and transverse energies are compared to those of a calculation based on intranuclear cascades followed by an evaporation step. The trend of the distributions are very similar confirming the importance of prompt emissions in experimental data.

Keywords: Intermediate energy, $^{36}Ar+^{58}Ni$ reaction, E=95 A.MeV. 4π multidetector INDRA, mi-rapidity emission Intranuclear cascade, percolation and evaporation calculations

PACS: 24.10.-i, 25.70.-z

Introduction

Heavy ion collisions at intermediate energies have revealed a lot of simple and paradoxally also complex phenomena explained by the fact that this energy domain is located between the low energy regime where the mean field is predominant and the high energy domain where two-body collisions prevail in the interaction mechanism. Above 200 A.MeV, the mean field being no more sufficient to retain together, during a suffisant time, the two partners; fusion, as well as binary deep inelastic process, are inhibited. This leaves place to the so-called participant-spectator scenario where in the outgoing channel two rather cold projectile and target remnants are accompanied by a hot piece of nuclear matter between them (the participant zone or fireball [1]). In the intermediate energy regime (30-100 A.MeV) where the cross of the Fermi energy can give hope to observe exotic phenomena, numerous experimental heavy ion collision studies have been carried out. Predominance of binary collisions or onset of the participant-spectator mechanism were claimed without indiscutable evidences [2].

For the present studied system Ar+Ni at 95 A.MeV [3,4], neighbouring ones [2] or heavier ones [5–10], a rather large contribution of the binary scenario is indeed observed. However when trying to follow this strict scenario a lot of intriguing features give rise to some doubts. How exchanges of nucleons, leading to high excitation energy, result in a small net mass

transfer and leaves each partner in thermal equilibrium? Deviations from this pure binary picture have already been observed [11] and theoretically predicted [12]. Some characteristics, particularly an estimate of the number of particles between the two main fragments and their mean transverse energies [13], are appealing for theoretical interpretation. Indeed the intermediate velocity contribution relative to the total mass of the system appears independent of the bombarding energy but is strongly dependent on the violence (geometry) of the collision [13–15]. Mechanisms like neck formation and rupture between the two fragments, extreme deformation for one of them, formation of hot spots, etc ..., have been proposed to explain this particularity . This could be also interpreted as a reminiscence of the high energy regime where the participant zone is thought to be separated from the two spectators. Another interesting aspect is the mean transverse energy of these intermediate velocity emissions which is higher that the one of the particles which are less ambigously identified as evaporative particles from the projectile and target-like fragments. This could be interpreted as a third intermediate source (fireball) hotter than the two main remnants (spectators). The apparent geometrical influence reinforces the hypothesis that the regime of high energy is already achieved.

The intranuclear cascade (INC) calculations are the simplest treatment of the nucleus-nucleus interaction at relativistic energy [16–19]. They showed good agreements with the Bevalac data in the 80's and have refound large interest with the advent of Accelerator Driven System project in the recent years [20,21]. In this paper we will apply the nucleus-nucleus INC model plus percolation [22] followed by an evaporation code [23] to the system Ar+Ni at 95 A.MeV. Although the studied energy domain is rather low in order to satisfy the INC model oversimplifications, we will compare the overall behaviour of the data with the present model. In section I the intranuclear cascade calculation will be presented. The percolation procedure (section II) and the evaporation code (section III) will next be described. Finally comparisons between data and calculations will be shown in section IV.

I. INTRANUCLEAR CASCADE MODEL

The Liège INC model first developed in [19] has been used with the percolation approach presented in [22]. Recent improvements mainly on parameterisation of nucleon-nucleon interaction cross sections are described in [24,25]. Most of the details on the Liège INC model are given in [19]. The version used here modelizes the full nucleus-nucleus interaction. It includes pions and deltas as well as isospin degrees of freedom. At first the nucleons inside each nucleus are positioned at random in a sphere of radius $1.12A^{1/3}$ (where A is the nucleus mass) and in a momentum space sphere of radius P_F=235 MeV/c to account for the Fermi momentum. The Fermi motion of nucleons is frozen up to the first collision. The impact parameter (b) of the collision is randomly chosen in a disk of radius equal to the sum of the radii of the two nuclei. The calculation uses relativistic kinematics and particles are moving along straight line trajectories until two of them reach a minimal distance of approach governed by the total collision cross section where they can interact. Soft collisions, as they are mainly forbidden by the Pauli principle, are suppressed to shorten the time calculation; for the present low bombarding energy, the collisions are allowed down to 35 MeV. For other collisions, the Pauli principle is applied to forbid final states already occupied. This blocking factor relies on phase space occupation probabilites inside reference volumes in radial-space of 2 fm radius and in momentum space of 200 MeV/c radius around each particle in the final state. The binding energies of the nucleons in the nuclei are neglected. The absence of potential, avoiding treatment of collisions of nucleons off their mass shell is justified at high bombarding energies. Here it will be restored in a rather crude manner as explained in the following subsection.

All the particles are followed in time up to a stopping time discussed below. Since the colliding nuclei are treated as a cloud of nucleons, no fragments are existing at the cascade stopping time. At that time (see subsect. I.B), a percolation procedure (sect. II) is used to construct residual fragments. The radial space distribution is considered and two nucleons are attributed to the same cluster if their relative distance is smaller than a chosen

percolation distance. This uses the construction of a minimum spanning tree [26] based on the relative distances between nucleons. Links larger than the percolation distance are cut out. Nucleons which remain linked constitute the clusters.

A. Potential restoration

In order to restore in part the potential well to bind the nucleons in the nucleus, fact which can be of importance at the relatively low bombarding energy studied here, a procedure has been used in the present version of the model. Such an attempt has been also applied in [27]. Since the origin of each colliding nucleon is known (target or projectile), after each nucleon-nucleon collision the energy of the nucleon relative to its emitter is compared to a value V (here 32 MeV). Nucleons more energetic than V can escape, with an energy lowered by V, otherwise they reintegrate their parent nucleus waiting for an eventual new collision. This "potential" energy could be considered as the energy averaged over all the nucleons of a nucleus needed for a nucleon to escape from the potential well.

B. The choice of the stopping time

In the nucleon-nucleus collision treatments, the binding potential exists and besides the cascade particles, an excited residual nucleus is left at the end of the cascade. The INC stopping time has been parameterised [25] as a function of target mass, energy and impact parameter using criteria based on the evolution of various variables with time. Namely, excitation energies, emission anisotropies or saturation of the cumulative numbers of collisions or of escaping particles were studied. Changes of behaviour were observed at about the same time, so defining this stopping time to switch to evaporation regime. For the present situation the switching time from cascade to percolation is determined in a similar manner. Fig. 1 (a) shows, for the Ar+Ni system at 95 A.MeV, the evolution of the cumulative number of colliding baryons versus the development time of the intranuclear cascade for different impact parameters. One can remark that at a given time, the number of collisions increases

with centrality of the collisions. However one observes also a saturation around 40 fm/c whatever the impact parameter is. Performing our method to take into account a binding potential does not change very much the picture. The number of colliding baryons (open symbols) slightly decreases because some of the low energetic scattered nucleons have been reattributed to their emitter.

Hence the time to switch on the percolation has been chosen to 40 fm/c. Another criterion has been added to avoid spurious cluster formation since the system is propagated only when a collision occurs. In Fig. 1(b) the time of the last collision versus the impact parameter is presented. It appears that for peripheral reaction where only few collisions occur, the stopping time is small and the percolation wrongly aggregated all nucleons. To avoid this, the propagation was continued up to $t_{final} = \frac{3}{4} * (40 - t_{last})$ where t_{last} is the time of the last collision. Fig. 1(c) shows the final time after correction. In Fig. 1(d) the mean position in the beam direction for non-interacting projectile nucleons is presented for the uncorrected (circles) and corrected (squares) final time as a function of the impact parameter. One observes that the time adjustement allows to have a monotonic evolution of the mean position with the impact parameter. Thus it is possible to perform the percolation with good initial conditions.

II. PERCOLATION PROCEDURE

A. The choice of the percolation parameter

The minimum spanning tree [26], used to construct fragments, is based on the relative distances between nucleons at the end of the cascade. The breaking of links implies a choice for the maximum distance (the squared distance d_{cut}) to allow cluster formation. In reference [22], this distance was phenomenologically chosen at 4 fm^2, a value reasonable in regard to the average inter-nucleon distance in nuclear matter. It was also pointed out that ambiguities exist between the choice of that value and of the stopping time. The value t_{stop} was fixed

here with the above criteria including a certain dependence with the impact parameter (see Fig. 1(c)). A test on transparent reactions revealed that the d_{cut} value had to be adjusted according to the impact parameter. Such a dependence has been also used in [27]. Indeed, switching the collisions off and propagating nucleons up to the t_{final} value found in Fig. 1(c), the d_{cut} value was adjusted to still observe projectile and target after percolation. For central collisions the d_{cut} value was evaluated to 4 fm^2 and for peripheral collisions a value of 8 fm^2 was found. Switching the collisions on, the values had to be lowered to 3 fm^2 for central collisions and to 8 fm^2 for peripheral ones to minimize the number of fusion events not seen experimentally. This d_{cut} adjustement can be interpreted as a compensation required by the fact that percolation is performed only in R space. The momentum dispersion being smaller for peripheral collisions, a larger R dispersion is allowed. Finally, these choices have to be justified a posteriori when comparing to the experimental data.

B. Results of the INC+percolation calculation

Main basic results of the intranuclear cascade + percolation are displayed in Fig. 2 and 3. The mass distribution shown in Fig. 2(a) exhibits a small contribution of fusion events at masses ~90 with target (A=58) and projectile (A=36) remnants. In (b), (c) and (d) the mass distributions are depicted for three different impact parameters. For central collisions we observe a continuously decreasing distribution, while for mid-central reactions the reminiscence of the quasi-projectile (QP) and quasi-target (QT) fragments begins to appear and is finally predominent for peripheral collisions. Most of fusion events for mid-peripheral collisions are unrealistic. Indeed, for some events a small number of scattered nucleons are located between the QP and the QT at such a distance that their links are not cut by the percolation. Although the mass ot the compound is important, the nucleon distribution in the R space is completely distorted. Since the contribution of these events is small (less than 1%) , they will simply be rejected. Fig. 3(a) shows a calculated bidimensional spectra of the maximum charge (Z_{max}) as a function of the impact parameter,

Z_{max} being the greatest charge with a rapidity larger than half the projectile rapidity ($Y_{Z_{max}} \geq Y_p/2$). One can observe a gentle relaxation in mass of the quasi-projectile with the decreasing impact parameter down to 4 fm and then a faster fall off.

The fragment excitation energy is the sum of the total energy of nucleons inside the fragment minus the total (kinetic + mass) energy of the fragment. An extra excitation energy was added in this version of the code. Indeed, the way the potential is restored does not conserve energy. Then, it is assumed that nucleons which had not enough energy to escape the nucleus brought a certain amount of excitation energy to their parents. This quantity (δ E) is given by $Nin_f \frac{E_{ini}-E_{fin}}{Nin_{tot}}$ where Nin_{tot} is the total number of nucleons not able to escape in the whole system, Nin_f the nucleons included in a fragment f which were not able to escape and E_{ini} and E_{fin} the initial and final total energy of all nucleons. This correction is applied to fragments of charge greater than 6. This procedure permits to avoid part of the energy conservation violation implied by the method described in subsection I.A. The calculated excitation energies per nucleon as a function of the fragment charges are shown in Fig. 3(b) and the mean values (dots) are superimposed. The two major contributions correspond to projectile ($Z \leq 18$) and target remnants ($Z \leq 28$). For fusion events, the excitation energy is particularly high. The low probability of these events makes useless a particular treatment and these events will be rejected. In Fig. 3(c) the mean excitation energy for the heaviest QP (QP_{max}, squares) and QT (QT_{max}, circles) residues are shown. The attribution of the remnant fragments have been done with velocity selection criteria ($Y/Y_p >(<) 0.5$ for QP (QT)). One observes rather low values increasing when the remnant masses are decreasing. As expected this variation illustrates the increase of relaxation when the primary masses move off the incident masses. The insert in Fig. 3(c) shows the correlation between QT_{max} and QP_{max}. The achievement of the excitation energy sharing between QP and QT can be inferred from these two graphs.

After intranuclear cascade and percolation the outgoing channel is composed of fragments and free nucleons, production of pions being marginal at the studied energy. The free nucleons can be viewed as the so-called preequilibrium particles. The characteristics of the

free protons are shown on Fig. 3(d). The full histogram represents their rapidity distribution in the laboratory frame, normalized to the projectile rapidity, integrated over all impact parameters. It is peaked at the reduced rapidity equal to 0.5 as expected in nucleon-nucleon single collision. Due to multiple collisions and to Fermi motion distribution, the spectrum extends largely beyond the target and projectile region (Y/Y_p=0 and 1 respectively). This extension is in qualitative agreement with the velocity distribution of dynamically emitted particles predicted by a semiclassical transport model [12]. The dots on Fig 3(d) is the variation of the mean transverse energy ($E_{tr} = m_o c^2[\sqrt{1-\gamma^2\beta_\perp^2} - 1]$) versus the reduced rapidity. In a single nucleon-nucleon collision one would expect a maximum of the $<E_{tr}>$ value of E/4 where E is the incident energy. Multiple collisions, the percolation procedure which could tend to aggregate the lowest energetic nucleons and rejection of soft collisions to respect the Pauli principle render this maximum value somewhat larger ($\sim$27 instead of 23.75 MeV).

III. EVAPORATION

Besides the free nucleons, light composite particles and excited fragments are present in the exit channel. The excitation energies imparted to the different outgoing charges shown on Fig. 3(b) have to be evacuated by means of an after burner. The evaporation code of Dresner [23] has been used. It is commonly employed in large code systems like HETC and LAHET [28,29]. It calculates the statistical decay of the fragments following the formulation of the Weisskopf theory [30] based on the detailed balance for the light particles (n, p, d, t, ^{3}He, ^{4}He). The angular momentum is neglected. The level density parameters were those from [31]. Instead of standard evaporation formula for light fragments of mass $\leq$ 21, the code uses the Fermi breakup [32] model.

IV. COMPARISONS

Experimental data were obtained with INDRA [33], a 4π multidetector for charged particles. The experiment was performed at the GANIL facility which provided an ^{36}Ar beam of 3-4 x 10^7 pps at 95 A.MeV. A minimum bias trigger required a four fold event. Charge identification is achieved up to the projectile charge in the forward hemisphere. Hydrogen and helium isotopes are separated for detection angles from 3^0 to 176^0. For spectra presented here, software energy thresholds were fixed at 2 A.MeV for hydrogen isotopes and 1 A.MeV for helium isotopes to homogenize the data in the whole detector. Angles are chosen randomly inside the limit angles of each ring of the detector, these rings covering 2π at fixed polar angles.

Experimental and calculated fragment characteristics are compared in Fig. 4 and 5. Fig. 4(a) shows the correlation between Z_{max}, the heaviest fragment in the forward hemisphere, and the impact parameter. As shown in Fig. 3(a) and 4(a) a fair correlation exists between Z_{max} values and the impact parameter. The decrease of Z_{max} with the impact parameter is smoother in the full calculation. Hence, Z_{max} can be used to classify the events according to the violence. The lowest Z_{max} are associated to the most central processes and the Z_{max} values near the projectile charge to the peripheral interactions. Fig. 4b) shows the experimental (full line) and calculated Z_{max} distributions. Particularly one notes the depletion around Z_{max}=9 produced by the small number of stable isotopes of this element. A reasonable agreement in shape can be observed.

In the left part of Fig. 5 are compared the laboratory rapidity spectra for different Z_{max} values. A fair agreement is also obtained but calculated spectra exhibit a smaller relaxation as well as a narrower width than the data. The absence of the mean field in the calculation could probably explain this discrepancy. Angular distributions for the same Z_{max} values are compared on the right panel of Fig. 5. As in the data, an angular cut of $\theta \leq 2^o$ has been applied to the calculations. A good agreement is observed except for the more peripheral collisions. In the following, Z_{max} will be used to classify the events according to the violence

of the collision, both in experimental data and calculations with this angular cut. For light particles, experimental biases like angular cuts and the energy thresholds and limits are taken into account.

On Fig. 6, are presented the total charge and the multiplicities of different light charged particles integrated in the mid-rapidity region ($0.4 \leq Y/Y_p \leq 0.6$) (left panel) and integrated over the whole rapidity range (right panel) as a function of Z_{max}. Since the aim of this study was the comprehension of the mid-rapidity components, we comment first the left part of Fig. 6. In the upper part the sums of charges (essentially light charged particles) in the region $0.4 \leq Y/Y_p \leq 0.6$ are compared. The calculations agree with the data although predicted values slightly overestimate the experimental ones. Thus this shows that for this particular region of interest the model is well suited. The individual light particle multiplicities in the mid-rapidity region are also compared. The calculated multiplicities are shown before and after the evaporation stage. One can notice that the evaporation step has a small influence in this region. For all light species the predicted trend of the variation of the multiplicites versus Z_{max} follows rather well the experimental behaviour. However there is an overestimation of the proton multiplicities. One can notice that the deuterons and in a lesser extend the ^{3}He are well reproduced. For tritons and mainly for the alpha particles the calculation underestimates the multiplicities. The same observables are compared for the full rapidity range on the right part of Fig. 6. One observes still a good agreement for the total charge and also for the individual multiplicities. The general trend is well reproduced. One can remark that the evaporative contribution becomes rather important and that the reproduction of the data is of the same quality as for the mid-rapididy region. The excess of protons could be related to the underestimate of alpha particles. It seems that too many free protons are left after the percolation since after this stage already theoretical predictions reach the experimental values. Hence we could infer that percolation does not build enough clusters. This is also an observation done in a recent work [34] using the intranuclear cascade code ISABEL [17] complemented by a coalescence procedure. This study restricted to the mid-rapidity component shows also difficulties to build enough clusters. The treatment of

the aggregation process is still an unsolved problem on which further theoretical works are needed. Another part of the discrepancies for ^{4}He could be due to the evaporation code itself which is known to underestimate alpha production for light systems [35]. However, the use of the GEMINI code [36] leads to about the same trends. Since the production of heavier particles is more sensitive to the angular momentum, the neglect of it could also explain part of the discrepancy. The prediction of the relative production rate can depend on the various default parameters used in the evaporation codes which could not be very well tuned for the present large spread of excitation energies in residual nuclei. The kinematical properties could be a better test of the potentiality of the present model.

On Fig. 7 the calculated (grey lines) proton laboratory rapidity distributions (left) are compared to the experimental data (black lines) for some Z_{max} values. The spectra are normalized to the number of protons associated to each Z_{max} value. The experimental shape is fairly well reproduced with a tendancy to slightly overestimate the mid-rapidity component. The contribution from pure intranuclear cascade (grey histograms) fills up nicely the mid-rapidity region and extends well above the projectile and below the target bumps.

The mean transverse energy (right panel of the Fig. 7) is an interesting variable which clearly signs the occurrence of the mid-rapidity emission [13]. The calculations (open symbols) exhibit as the data (full symbols) the presence of a plateau in the QP and QT region and a large peak at mid-rapidity. The $<E_{tr}>$ value in the QP and QT region increases from 5 MeV to 10 MeV for Z_{max} decreasing from 15 to 6. This variation which can be interpreted as a higher energy transfer when Z_{max} diminishes is well reproduced by the calculation. The global trend of the $<E_{tr}>$ curve is well accounted by the calculation. However the peak at mid-rapidity is located at somewhat higher reduced rapidity and the mean value is too large (25 MeV instead of 20 MeV) specially for the most peripheral collisions. The use of mean values could be an easy way to summarize the data but a more significant confrontation is presented in Fig. 8 where the proton transverse energy spectra in coincidence with different Z_{max} fragments are shown. Only the region of mid-rapidity ($0.45 \leq Y/Y_p \leq 0.55$) for pro-

tons is presented. The normalisation has been done on the total content of each spectrum. The slopes at high energies are nicely reproduced showing that the present calculations are able to simulate quite well the characteristics of the mid-rapidity particles. Only the low energy region below 10 MeV is underpredicted.

In Fig. 9, the deuteron rapidity distributions in the laboratory frame (left panel) and mean transverse energies (right panel) are presented. The agreement between experimental (black lines) and calculated rapidity distributions, although less satisfactory than for protons, is good. The mid-rapidity region is satisfactory reproduced but there is an overestimate by the calculations of the evaporative part in the QP region which is less apparent in the QT region. For transverse energies, the same discrepancy as for protons is observed. The mean calculated values at intermediate velocity are too high. One notes also that the excess of the evaporation part for deuterons lowers the mean predicted transverse energy in the QP region. However the general kinematical trend and the multiplicities (Fig. 6) are well reproduced.

V. SUMMARY

The mid-rapidity emission has been studied for the Ar+Ni reaction at 95 A.MeV. An intranuclear cascade+percolation model followed by an evaporation code reproduces the global behaviour of the reaction relatively well if one notices that the validity of such an approach is rather marginal in the considered energy range. A special emphasis has been put on the mid-rapidity emission since the physics of the participants is well suited to the treatment by the intranuclear cascades. The kinematics properties of this region which by no mean can be explained by treatments assuming thermalised emission from the projectile and target remnants are well reproduced by the present model. This shows that its simple physics inputs are able to describe the characteristics of the particles emitted in the velocity region between the target and the projectile remnants. They are attributed to prompt emissions before any equilibrium can be reached. Rather good descriptions of the QP and QT remnant properties like the trends of the mass and excitation energy distributions with

the violence of the collision are also obtained. More refined transport models could bring further quantitative agreements but they need at least to incorporate the simple ingredients present in the intranuclear cascade model.

REFERENCES

[1] J. Gosset, H. H. Gutbrod, W. G. Meyer, A. M. Poskanzer, A. Sandoval, R. Stock, and G. D. Westfall, Phys. Rev. C **16**, 629 (1977).

[2] R. Dayras *et al.*, Nucl. Phys. **A460**, 299 (1986).

[3] M. F. Rivet *et al.*, Phys. Lett. B **388**, 219 (1996).

[4] Y. G. Ma *et al.*, Phys. Lett. B **390**, 41 (1997).

[5] C. P. Montoya *et al.*, Phys. Rev. Lett. **73**, 3070 (1994).

[6] J. Tõke *et al.*, Nucl. Phys. **A583** 519 (1995).

[7] J. F. Lecolley *et al.*, Phys. Lett. B **354**, 202 (1995).

[8] Y. Larochelle *et al.*, Phys. Rev. C **55**, 1869 (1997).

[9] E. Plagnol *et al.*, Phys. Rev. C **61**, 014606 (1999).

[10] F. Bocage *et al.*, Nucl. Phys. **A** in press.

[11] J.E. Sauvestre *et al.*, Phys. Lett. B **335**, 300 (1994).

[12] Ph. Eudes, Z. Basrak, and F. Sébille, Phys. Rev. C **58**, 2003 (1997).

[13] T. Lefort *et al.*., Nucl. Phys. **A662**, 397 (2000).

[14] D. Doré *et al.*, submitted to Phys. Lett. B.

[15] Ph. Buchet, Ph.D. Thesis, Université de Caen, 1999, unpublished.

[16] K. Chen, Z. Fraenkel, G. Friedlander, J. R. Grover, J. M. Miller, and Y. Shimamoto, Phy. Rev. **166**,949 (1969).

[17] Y. Yariv and Z. Fraenkel, Phy. Rev. C **20**, 2227 (1979).

[18] V.D. Toneev and K.K. Gudima, Nucl. Phys. **A400**, 173C (1983).

[19] J. Cugnon, Phys. Rev. C **22**, 1885 (1980).

[20] C. D. Bowman *et al.*, Nucl. Inst. Meth. Phys. Res. **A320**, 336 (1992).

[21] C. Rubbia *et al.*, CERN report CERN-LHC 96-011-ETT.

[22] J. Cugnon and C. Volant, Z. Phys. **A334**, 435 (1989).

[23] L. W. Dresner, Oak Ridge Report ORNL-TM-196 (1962).

[24] J. Cugnon, S. Leray, E. Martinez, Y. Patin, and S. Vuillier, Phys. Rev. C **56**, 2431 (1997).

[25] J. Cugnon, C. Volant, and S. Vuillier, Nucl. Phys. **A620**, 475 (1997).

[26] E. W. Dijkstra, Numer. Math. **1**, 269 (1959).
J. Dorfan, Z. Phys. **C7**, 349 (1981).

[27] G. Montarou *et al.*, Phys. Rev. C **47**, 2764 (1993).

[28] T. W. Armstrong and K. C. Chandler, Radiation Shielding Information Center, HETC Monte-Carlo Nucleon-Meson Transport Code, Report CCC-178, ORNL(1977) and Nucl. Sci. Eng. **49**, 110 (1972).

[29] R. E. Prael and H. Lichtenstein, Los Alamos National Laboratory Report LA-UR-89-3014(1989).

[30] V. F. Weisskopf, Phys. Rev. **52**, 295 (1937).

[31] A. V. Ignatyuk, G. N. Smirenkin, and A. S. Tishin, Sov. J. Nucl. Phys. **21**, 256 (1975).

[32] E. Fermi, Prog. Theor. Phys. **5**, 1570 (1950).

[33] J. Pouthas *et al.*, Nucl. Inst. Meth. Phys. Res. **A357**, 418 (1995).

[34] P. Pawłowski *et al.*, submitted to Phys. Rev. C.

[35] M. Enke *et al.*, Nucl. Phys. **A657**, 317 (1999).

[36] R. J. Charity *et al.*, Nucl. Phys. **A483**, 391 (1988).

FIGURES

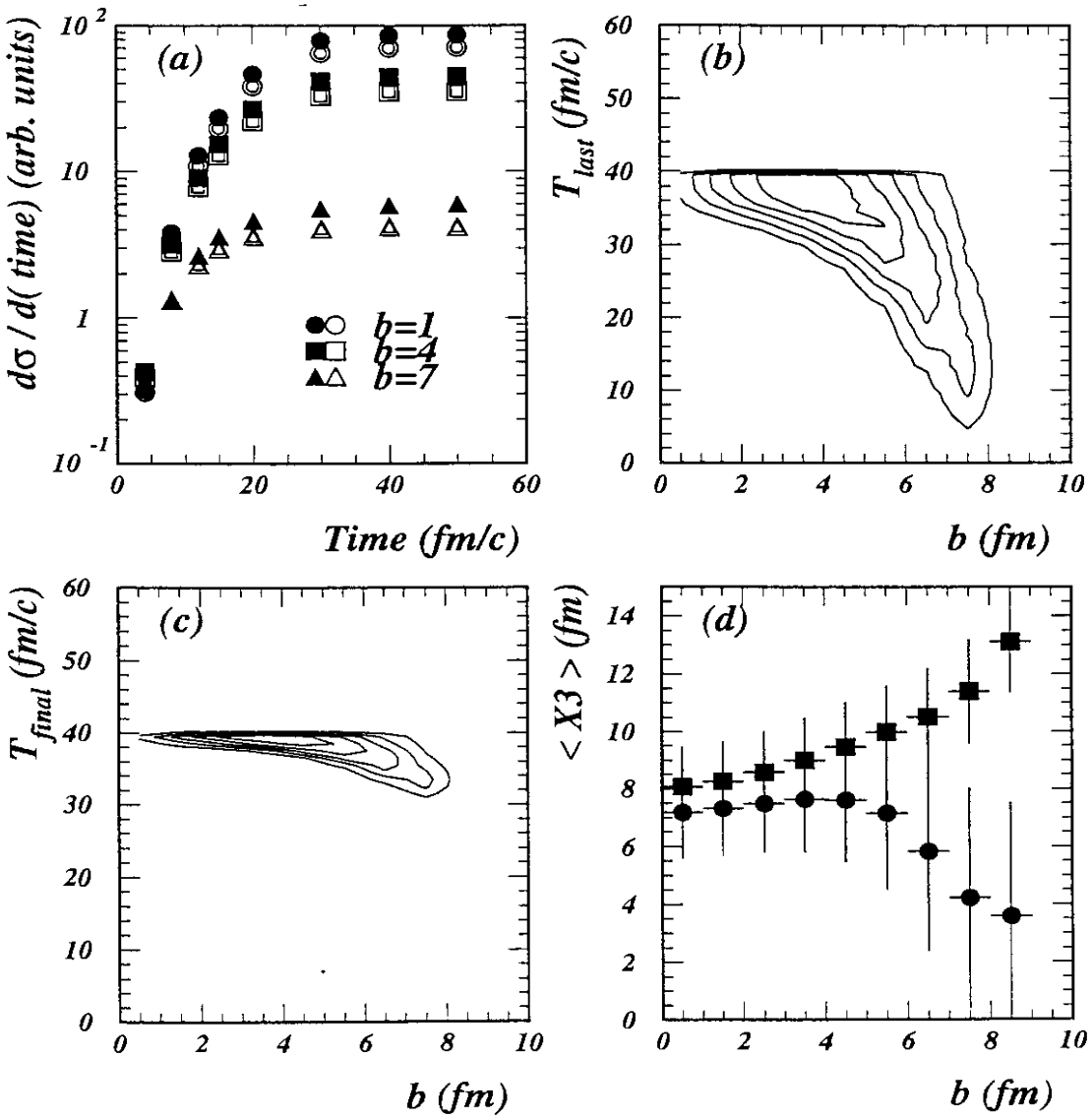

FIG. 1. Intranuclear calculation ingredients. (a) Cumulative number of hadron-hadron collisions with (open symbols) and without (full symbols) a simulated potentiel for different impact parameters as a function of the time. (b) Time of the last collision and (c) corrected final time as a function of the impact parameter. Contours in (b) and (c) are equidistant. (d) Mean position (parallel to the beam direction, the origin is the target) of the non-interacting projectile nucleons with (squares) and without (circles) correction of the end time.

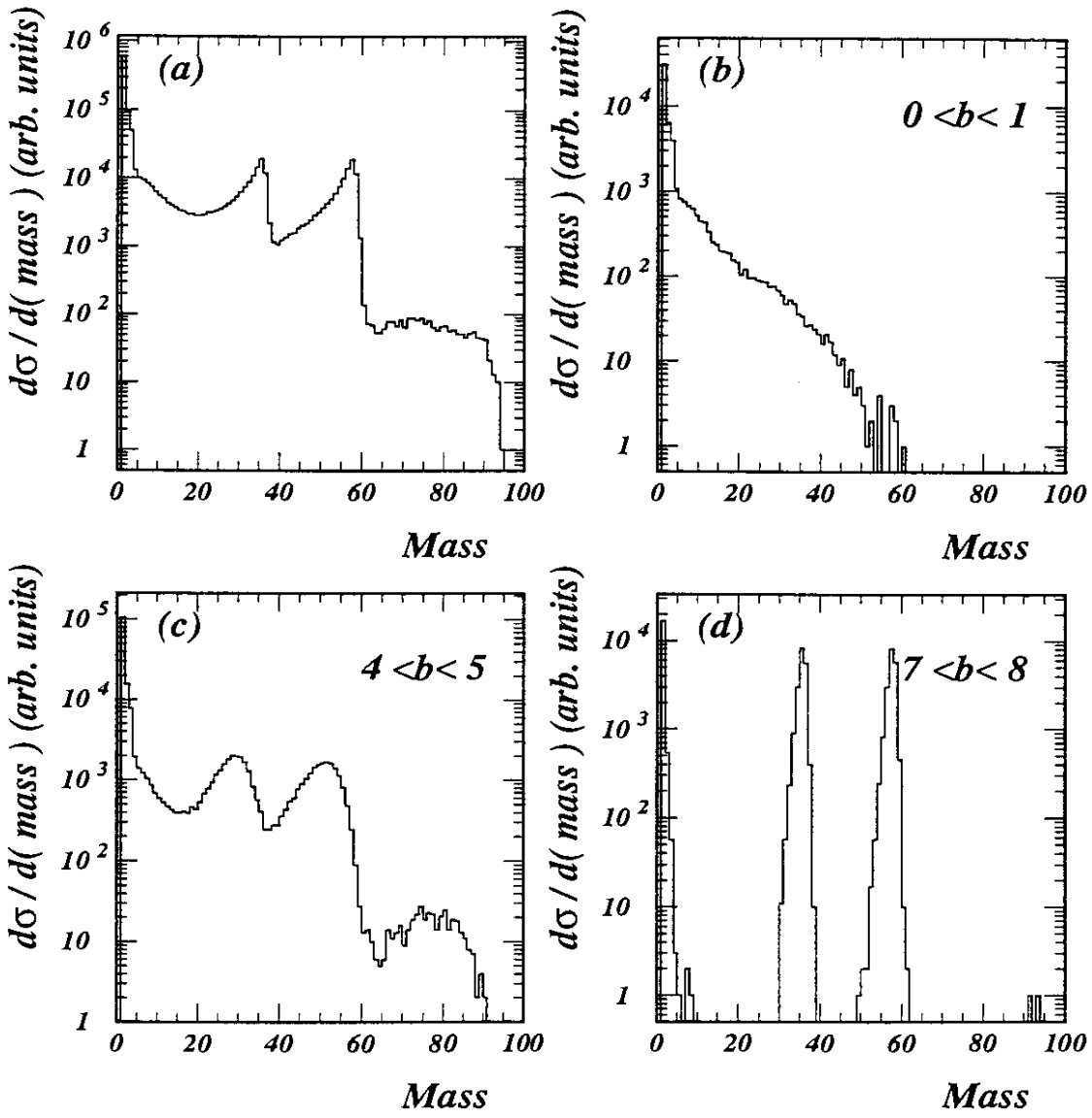

FIG. 2. Results of the intranuclear cascade and the percolation procedure. Mass distribution for all events (a), for central (b), midcentral (c) and peripheral (d) collisions

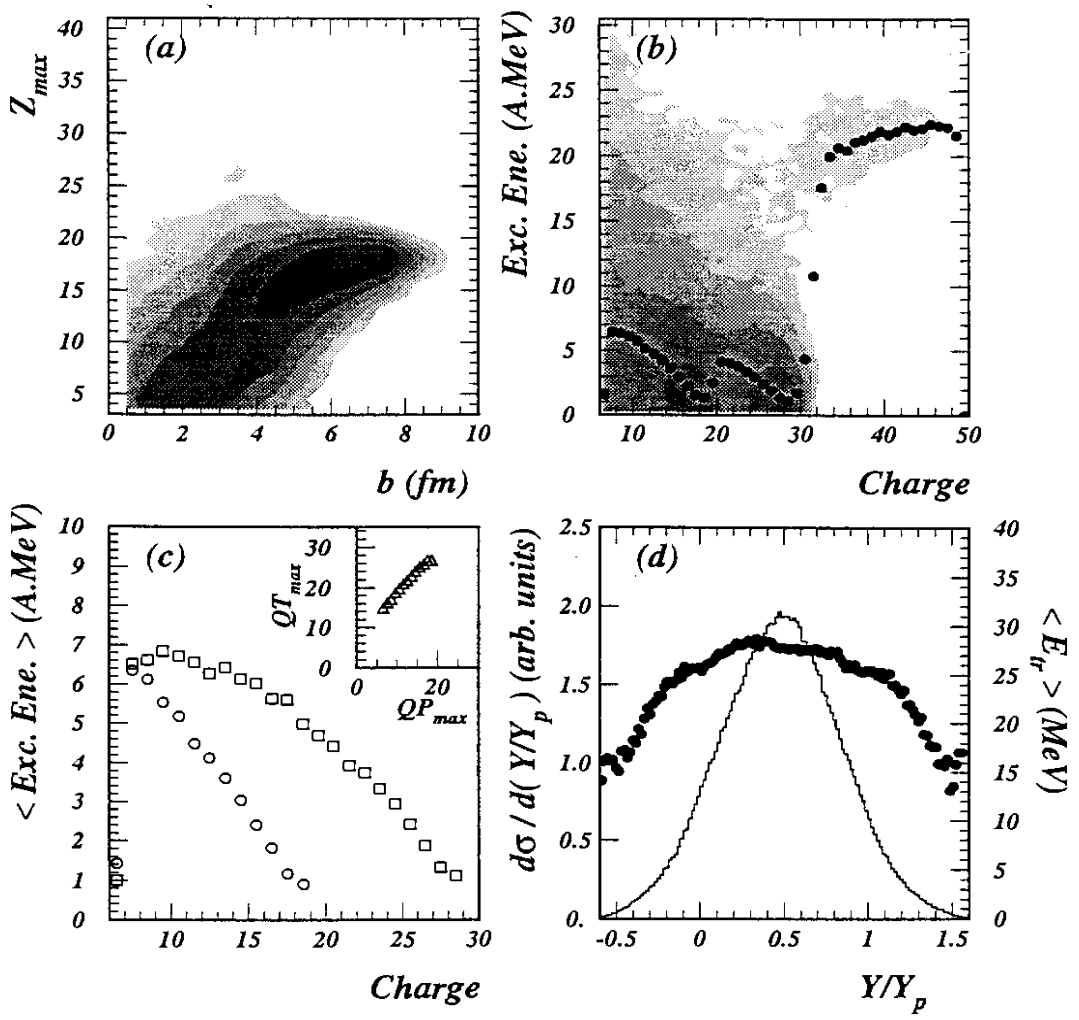

FIG. 3. Results of the intranuclear cascade and the percolation procedure. (a) Z_{max} (heaviest fragment in the forward hemisphere) versus the impact parameter. (b) Excitation energy as a function of the charge (points represent the mean value). There is a factor 5 between contour levels in the bidimensional plots (a) and (b). (c) Mean excitation energy for heaviest QP (circles) and QT (squares) residues as a function of the charge. The insert shows the correlation between the heaviest charges below (QT_{max}) and above (QP_{max}) mid-rapidity. (d) Proton rapidity distribution (left scale, histogram) and mean transverse energy (right scale, dots).

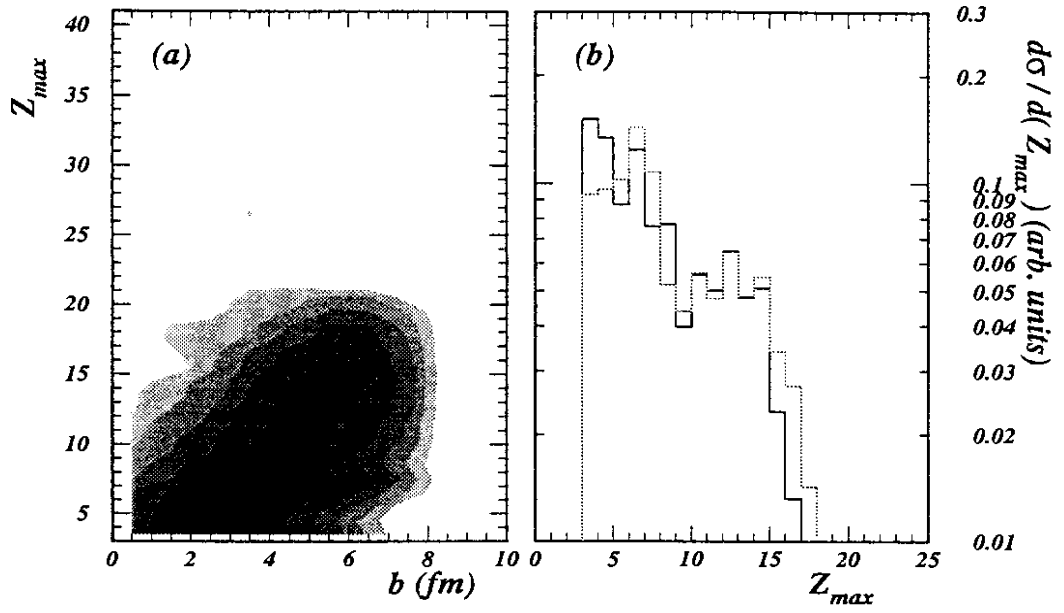

FIG. 4. Results of the calculations after intranuclear cascades + percolation + evaporation procedure. (a) Z_{max} versus the impact parameter b. There is a factor 4 between contour levels. (b) Calculated Z_{max} distribution (grey histogram) is compared to the experimental one (black histogram).

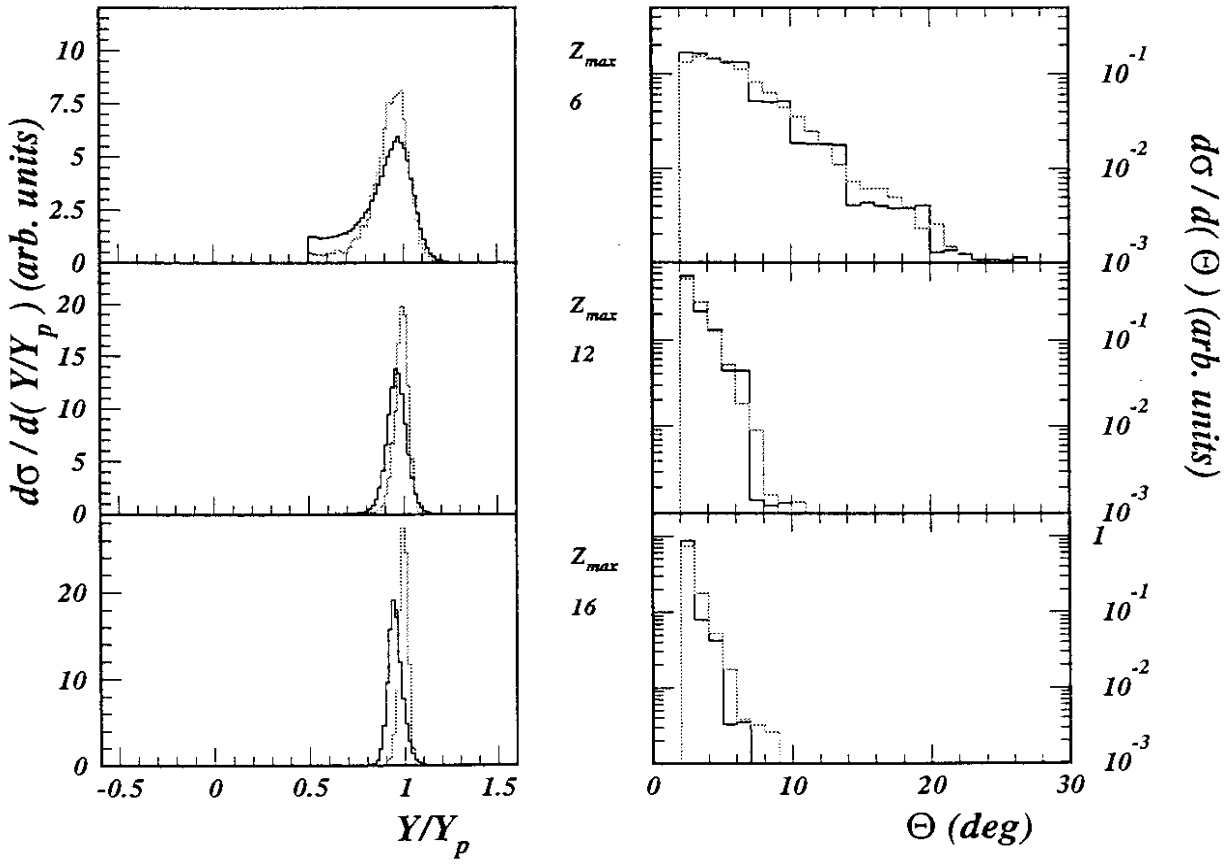

FIG. 5. Rapidity (left panel) and angular (right panel) distributions for $Z_{max} = 6$, 12 and 16. Black histograms are the data and grey histograms the calculations.

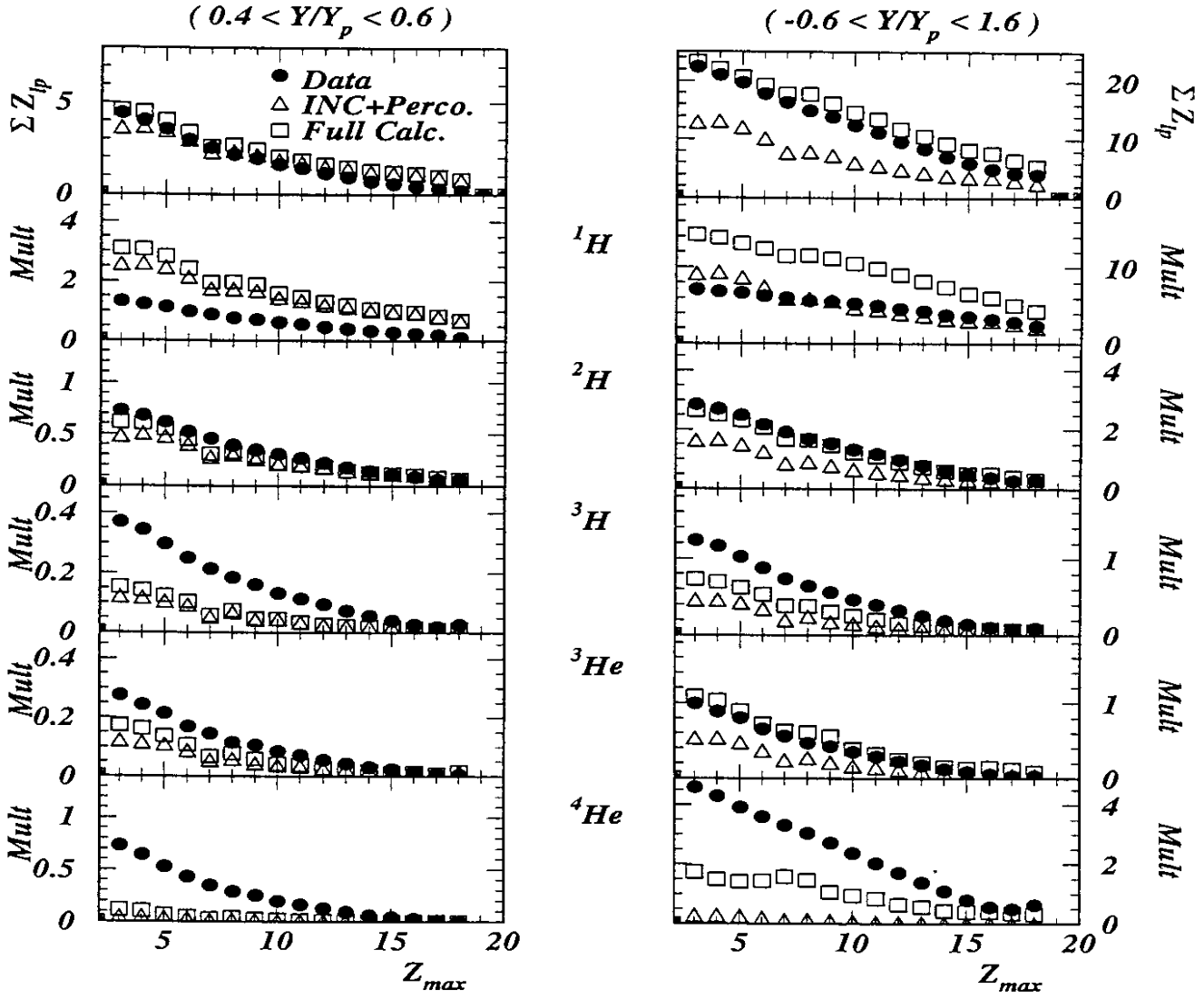

FIG. 6. Total charge and multiplicities of different light charged particles integrated in the mid-rapidity region ($0.4 \leq Y/Y_p \leq 0.6$) in left panel and integrated over all the rapidity range in the right panel as a function of Z_{max}. Filled circles represent data, triangles results of the cascade+percolation steps and squares results of the total calculation (cascade+percolation+evaporation).

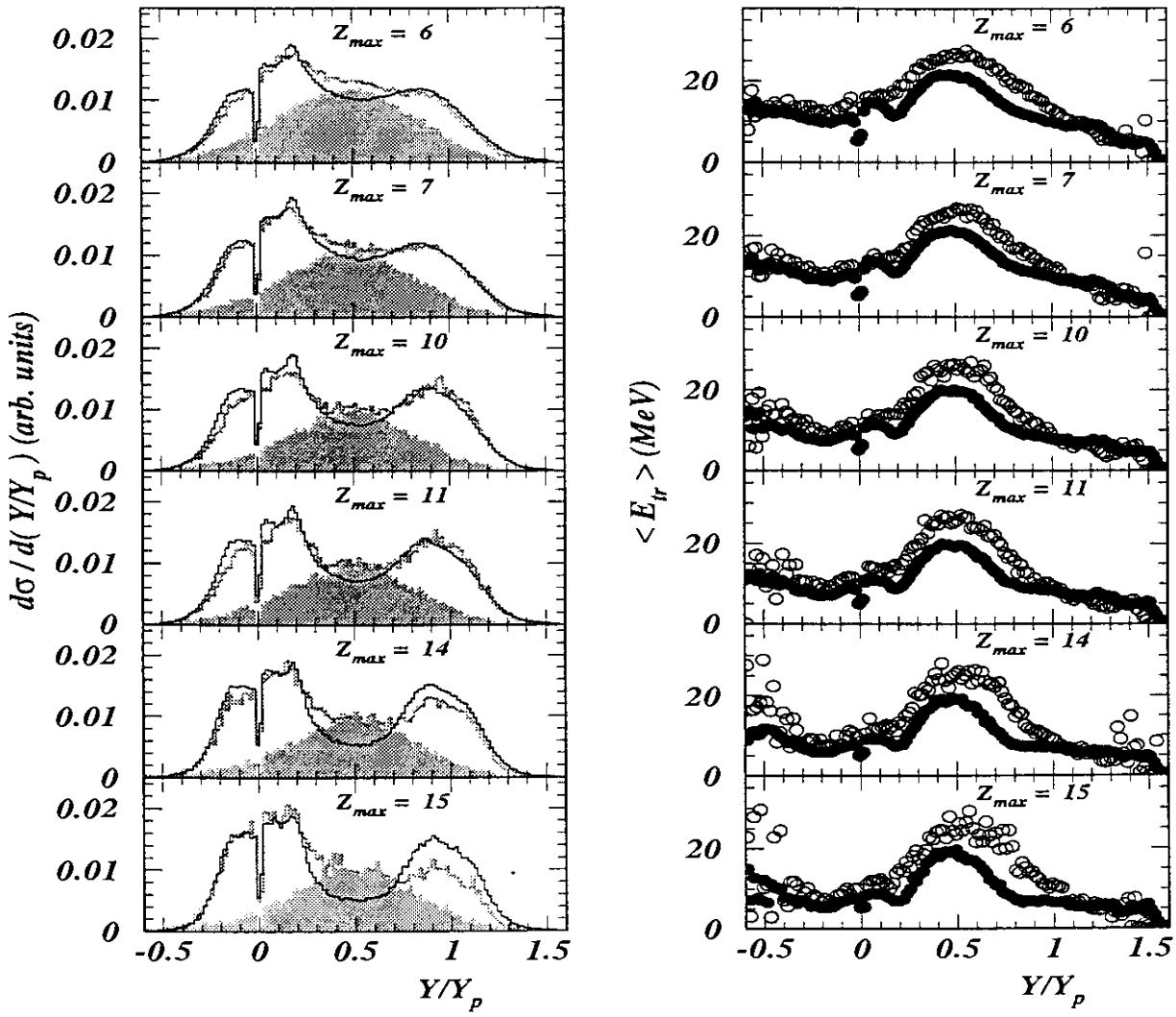

FIG. 7. For different indicated Z_{max} values ; Left : Proton reduced rapidity distributions, Right : proton mean transverse energy versus Y/Y_p. Data are shown with black lines and full symbols and calculations with open symbols, grey lines (full calculation) and filled histograms (INC + percolation).

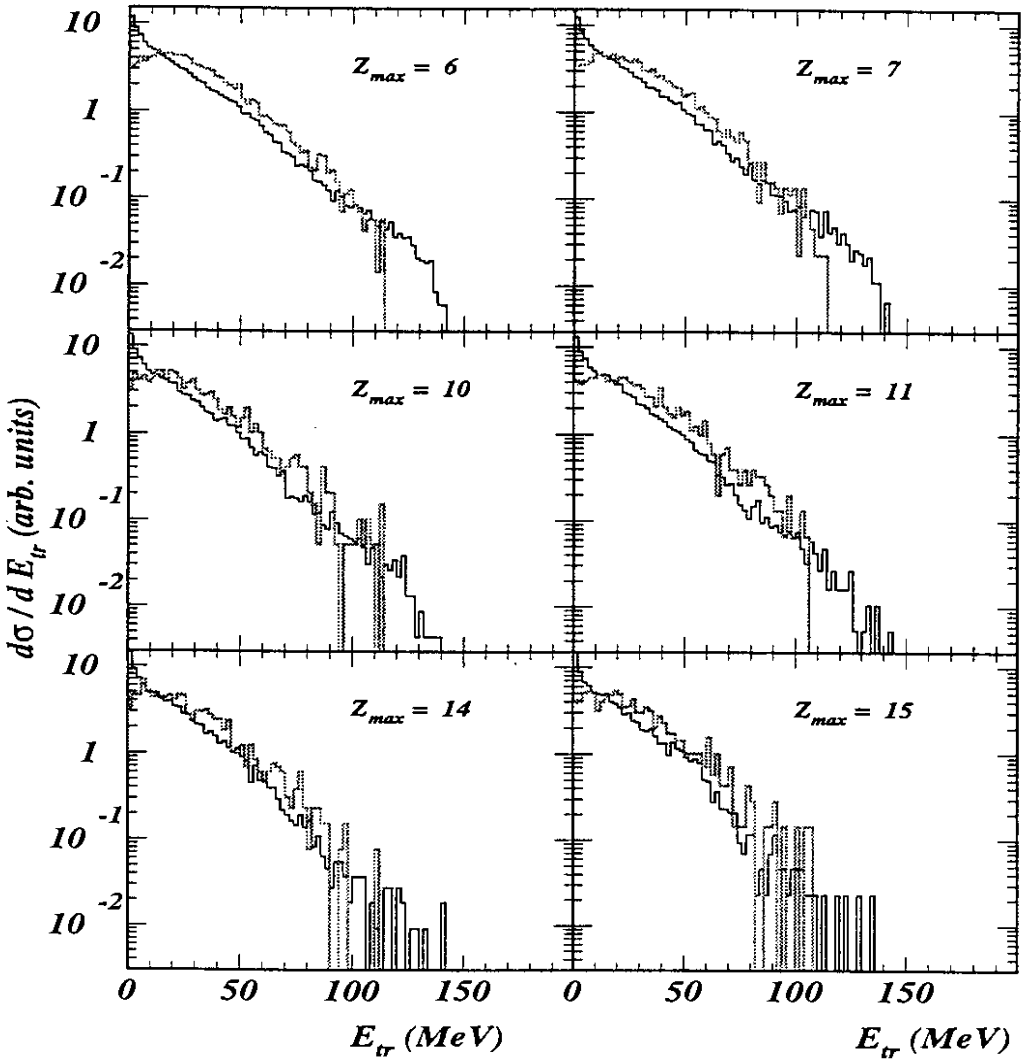

FIG. 8. Experimental (full line) and calculated (grey line) proton transverse energy distributions for few selected Z_{max} values as indicated. Protons with a reduced rapidity between 0.45 and 0.55 are selected.

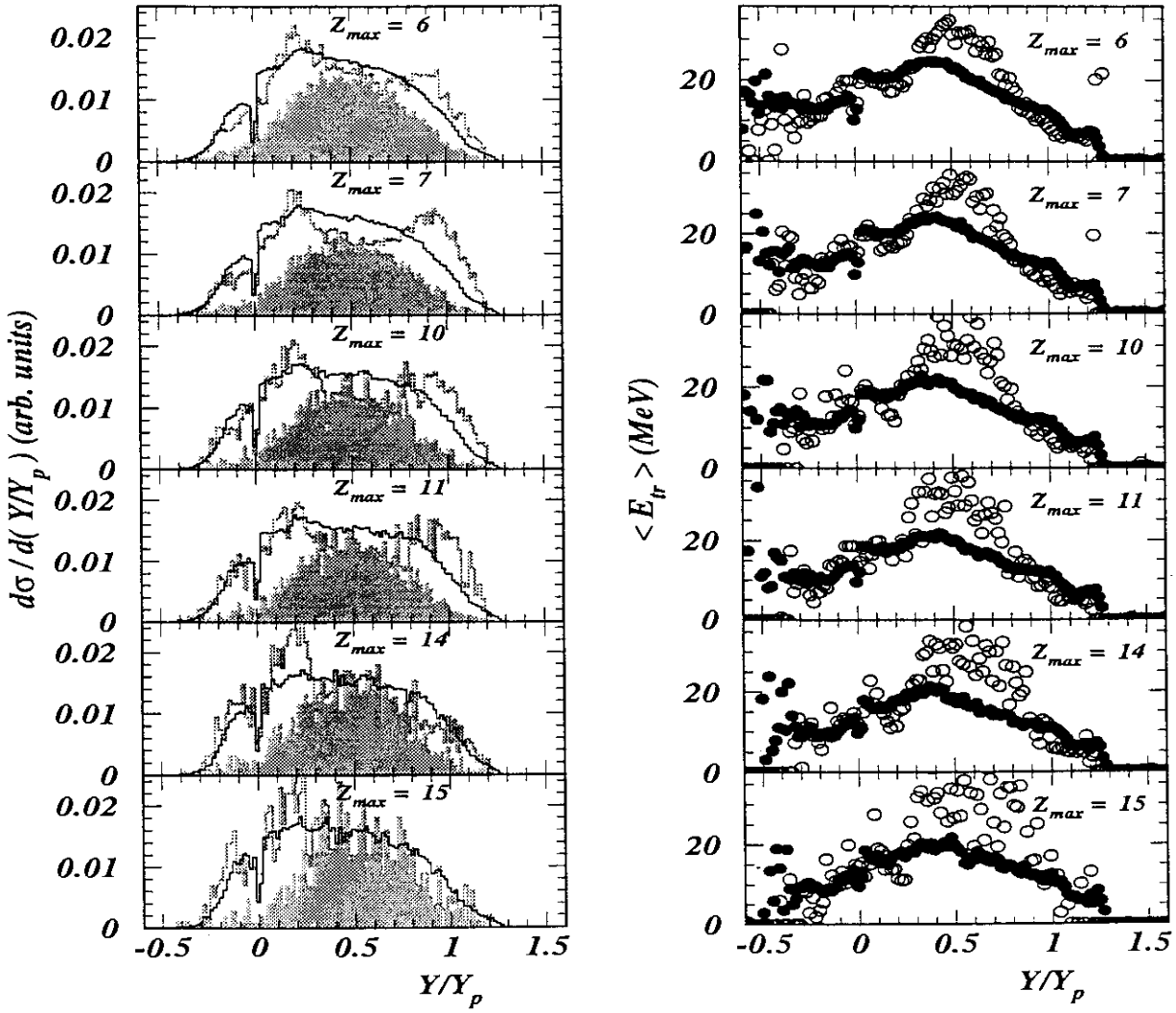

FIG. 9. For different indicated Z_{max} values ; Left : deuteron reduced rapidity distributions, Right : deuteron mean transverse energy versus Y/Y_p (see caption of Fig. 7).